

Chapter 2

Specimen Preparation

2.1 Introduction

In 1965 Müller, the father of the atom probe, once observed, “... the specimen itself is also the image-forming “lens” and the imaging ion beams originate at the specimen surface” [1]. In other words, the specimen is the primary optic of the atom probe microscope, and as such, specimen preparation forms a critical step in a successful atom probe tomography (APT) analysis. Controlling the tip size and its shape is essential for understanding and manipulating the ionic trajectories from specimen surface to detector.

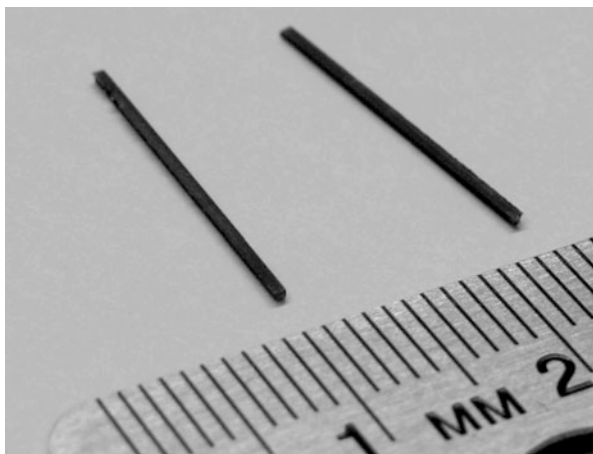
The motivation for nearly every specimen prepared for APT analysis is fundamentally the same: (1) the specimen must be sharp enough to allow field evaporation, (2) it must be robust enough to allow for significant evaporation events to occur, and (3) user-defined features of interest must be present in the near-apex region to ensure that such features are included in the collected data. Two main methods of specimen preparation are prevalent for APT: electropolishing and focused ion beam (FIB) milling, which are the focus of this chapter.

2.2 Electropolishing

There may be several reasons for electropolishing specimens. The method is relatively easy, often fast, and does not require expensive and complicated instrumentation. Often the user may not be interested in any specific feature but rather a more general survey of what is present in the microstructure (bulk analysis). Alternatively, the material may not be of interest at all but may serve as a generic test specimen that is necessary to evaluate some aspect of the LEAP instrument.

Until relatively recently (late 1990s), nearly all specimens prepared for APT were formed by electropolishing. Standard methods were transferred from electron microscopy [2] and applied to metals (though not exclusively) beginning with the

Fig. 2.1 Example of metal blanks with typical dimensions used for electropolishing



inception of high field work in the 1930s. General information on the techniques can be found in any reference book on the atom probe technique [3–9], and a large number of options for electropolishing and chemical polishing solutions may be found [2, 10].

If bulk samples do not already exist as wires, then blanks must first be cut from the bulk into appropriately sized pieces ($\sim 0.5 \times 0.5 \times 10\text{--}20 \text{ mm}^3$ is common). This can be accomplished by using a diamond or a rotating wire saw or by electro-discharge machining. An example of two finished electropolishing blanks is shown in Fig. 2.1. It is important that the cross section is square or circular in nature as asymmetric cross sections will lead to blade-shaped specimens that distort the ion trajectories toward the detector.

The first electropolishing step involves removing material from the middle of a blank in order to thin that region for separation and to form two roughly needle-shaped specimens. This is done using a simple setup as shown schematically in Fig. 2.2a. The blank is connected to a positive DC voltage (although AC is also often employed), and a metal electrode is connected to the negative polarity and placed inside a container with a dense inert liquid (such as Galden[®] PFPE heat transfer fluid) and a layer of electrolyte as shown in the schematic. The electrolyte layer should be just thick enough to be continuous. The inert liquid is optional, but dramatically reduces the volume of electrolyte required, and thus lowers storage and disposal costs. For many ferrous or nickel-based metals and alloys, the standard electropolishing solution used in this step consists of 10 % perchloric acid in acetic acid by volume (the user is referred to standard reference books for other electropolishing and chemical polishing solutions for various materials) [3]. The voltage is then switched on, and the specimen is manually moved up and down as indicated by the dashed arrow in the figure. During this stage, the sample may be easily held in locking tweezers or held by other mechanical means, while the sample blank thins down from its original diameter (the largest amount of thinning occurs in the center of the blank) and eventually separates into two pieces

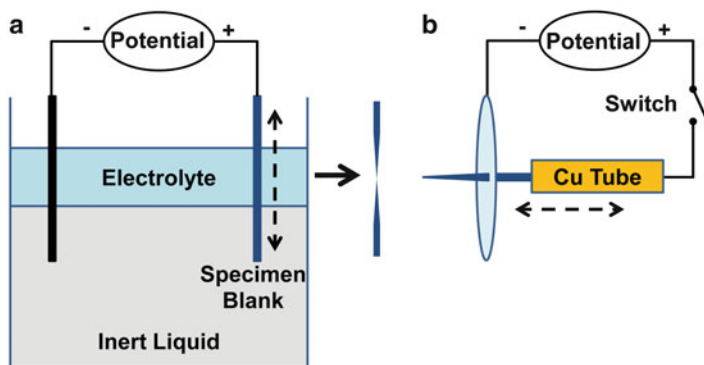


Fig. 2.2 Schematic of two types of electropolishing setups. (a) The suspended electrolyte setup consists of a relatively narrow film of active electrolyte floating on an inert liquid. A counter electrode is connected to the specimen blank via a potential difference. The specimen can be manipulated to control the electropolishing action (*dashed vertical arrow*). The process ends when the center of the blank necks until breaking (two-piece image immediately *right* of panel). This setup is typically used for rough polishing. (b) An alternative setup that provides the user with finer control includes a polishing loop that holds the electrolyte and is connected to the specimen via a potential difference which can be manipulated by motion of the specimen (*dashed horizontal arrow*) and gating of the electrical potential (*switch*)

as shown in Fig. 2.2a, right. At the completion of this process, both samples should be rinsed in distilled water and ethanol to remove any residual electrolyte and prevent deposition of any residue that might be dissolved in water remaining on the tip surface. The blank material can then be mounted into a small copper (or other metal) tube by crimping to enable easier handling and transfer for APT analysis. It should be noted however that after completion of this coarse polishing process, the specimens may not be sufficiently sharp for APT. This is accomplished in a second stage (often referred to as micropolishing), which is shown schematically in Fig. 2.2b.

The micropolishing stage forms the specimen into its final shape and may be accomplished in a variety of ways. The application of this step requires a dynamic application of voltage between electrolyte and specimen based on observed progression of the tip shape by the user [10]. The necking method, already described in the preceding paragraph, can also be used during the micropolishing stage but at a finer scale and with a smaller electrical potential. This procedure is used with the aid of an optical microscope, as shown in Fig. 2.3. The specimen, which has a very small shank angle, is positioned within a metal loop (negative polarity) filled with electrolyte as shown schematically in Fig. 2.4. A very fine neck is created in the specimen by moving the metal loop or the specimen back and forth (or up and down, depending on the orientation of the apparatus) in the loop and leaving a small region of the specimen outside of the loop (arrowed), Fig. 2.4b. For the final step of the procedure, the specimen is positioned as shown in Fig. 2.4c (with the loop well away from the necked region), the potential is switched on, and the specimen is

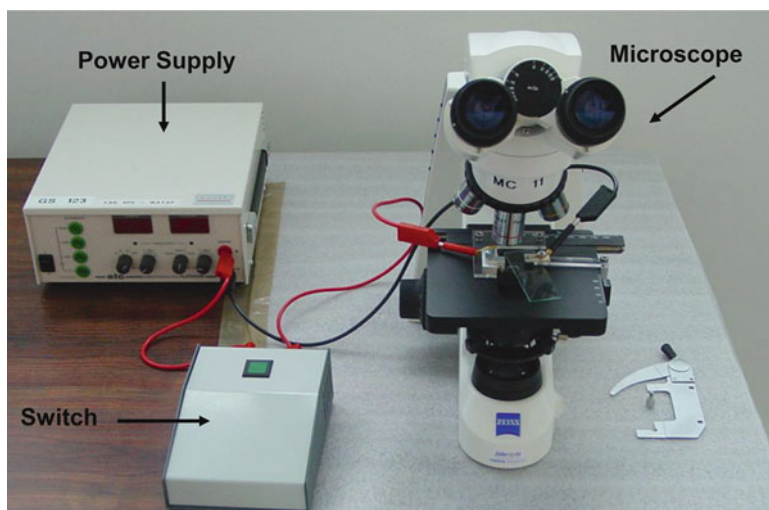


Fig. 2.3 Photograph of an actual electropolishing setup (also see Fig. 2.2b). The principal components include microscope, power supply, and switch (specimen and electropolishing loop are located beneath the microscope optic)

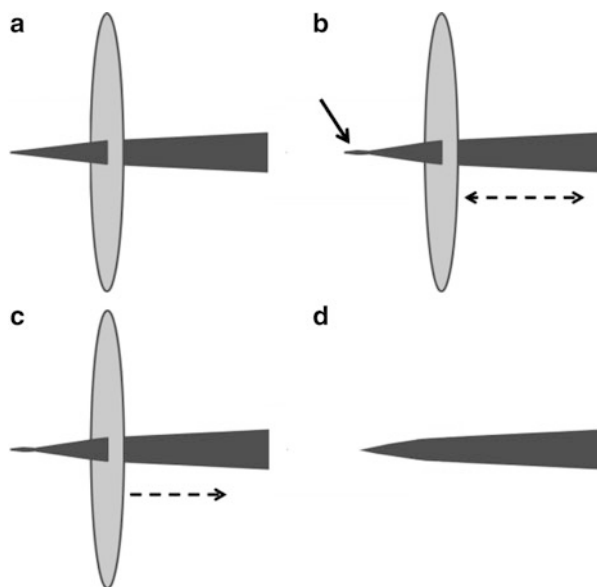


Fig. 2.4 Schematic illustrating evolution in the micropolishing procedure. (a) Initial placement of the electropolishing loop on a rough-polished specimen. (b) Typical motion of the loop (*dashed arrows*) which produces necking near the end of the tip (*arrow*). (c) Continued motion of the loop during application of the electric potential (*dashed arrow*) causing further necking near the end of the tip. (d) Final tip shape after the process has caused breaking at the neck

quickly withdrawn through the loop (dashed arrow in Fig. 2.4c). If the neck is not removed, the potential is switched off, the specimen is returned to the position shown in Fig. 2.4c, and the procedure is repeated until the neck is removed, leaving a completed specimen shape, Fig. 2.4d. Generally, the specimen is sharpest just after the neck has been removed, but this can be sharper than ideal for some low-evaporation-field materials. Additional iterations, similar to those described in Fig. 2.4c, can result in controlled blunting of the apex until the desired curvature is attained. Again, the specimen should be rinsed in distilled water and ethanol after the final shape is achieved. Following the end of APT data collection (either by blunting or fracture), needle specimens can often be repolished many times using the steps outlined in this micropolishing procedure.

In addition to the standard manual techniques, automated commercial instruments have emerged [11]. Simplex Scientific (Middleton, WI, USA) offers an instrument called the Electropointer that automatically prepares needle-shaped specimens with minimal user input. Once the starting wire or blank is inserted into the apparatus, the instrument automatically controls the voltage and current is applied to a small wire loop surrounding the specimen normal to its long axis. The loop is moved longitudinally by a stepper motor. All motions and electrical signals are controlled and monitored by computer. There is also an integrated light optical microscope that displays the magnified specimen shape during operation. The intent of this instrument is to take as input a coarse specimen blank and output a specimen that is ready for APT analysis. Feasibility for this approach has been shown for simple metals [11].

2.3 Needles Versus Microtips

The implementation of a local counter electrode in APT enables the use of microtip arrays or coupons as a means to quickly manufacture extracted material into APT-compatible specimens, an example of which is shown in Fig. 2.5. Microtip coupons offer numerous advantages over traditional needle geometry specimens [12]. The presence of many microtips per coupon makes it easier to collect a statistically significant number of datasets in a short amount of time, under very similar processing conditions, and without the need to cycle new specimens into the vacuum chamber. This improvement of speed and precision not only improves time to knowledge for typical applications, but it also allows implementation of a design-of-experiment methodology.

The microtip coupon shown in Fig. 2.5 contains an array of microtip specimen carriers oriented normal to the wafer surface. This provides a common height for all the tips and offers two additional advantages: (1) APT analysis through multilayer films is normal to the wafer surface (each carrier tip has exactly the same orientation, whereas a group of needles are not guaranteed to be identically straight), and (2) it minimizes ion beam realignment when moving among specimens when FIB

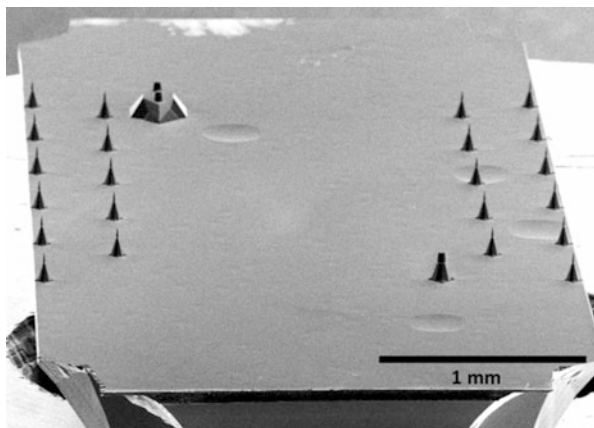


Fig. 2.5 SEM image of a microtip array (coupon). The coupons are 3 mm \times 7 mm with Eleven carrier microtips positioned along two of the edges (22 carrier tips total). Three additional large markers are visible more toward the middle of the coupon. These indicate sides 1 and 2 for reference purpose

sharpening multiple specimens (required when carrier tips are not identical in orientation and height).

Pre-sharpened microtips [13], with a tip radius of curvature ≤ 50 nm, offer an additional advantage in that they do not require FIB sharpening. This array type is designed to be run as a calibration standard for evaluating instrument performance or to serve as a substrate for deposition of films for APT analysis. Elimination of the need for any FIB processing also alleviates the detriments associated with gallium contamination and knock-on or ion-mixing damage of the stack during FIB sharpening [14] but with the caveat that the films are deposited on a highly curved surface. Furthermore, the samples are ready for analysis immediately upon completion of film deposition.

2.4 Electrostatic Discharge Considerations

The sharp tip geometry that makes it possible to produce electric fields sufficient to field evaporate material from APT specimen surfaces also makes the tips susceptible to undesirable electric field-induced issues during handling and transfer. Electrostatic discharge (ESD) is a single-event, rapid transfer of electrostatic charge between two objects, usually resulting when two objects at different potentials come into direct contact with each other. ESD can also occur when a high electrostatic field develops between two objects in close proximity. ESD is a common problem in the microelectronics industry, and well-known steps can be taken to minimize the potential for transfer of static charges to an APT specimen and to protect insulating specimens from natural fields and voltage differences that

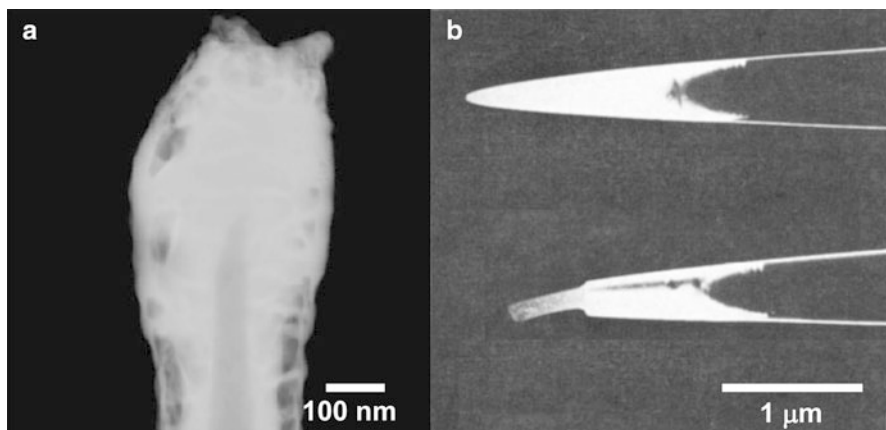


Fig. 2.6 TEM images of a tungsten tip that has been modified due to electrostatic discharge. (a) STEM-HAADF image showing amorphous WO_x layer surrounding W core material deposited through an ESD event (reprinted with permission from Cambridge University Press [16]). (b) Stainless-steel specimen tip as polished (*upper*) and after ESD (*lower*). The outermost part of the tip has disappeared and an amorphous outgrowth formed on the truncated tip (reprinted with permission from IOP [17])

may cause damage [15]. Besides destruction of the APT specimen from a discharge event between a specimen tip and its surroundings, ESD has also been observed to initiate blunting, sometimes in conjunction with the growth of amorphous material [16–18], Fig. 2.6.

Figure 2.7 shows TEM images of specimens that have not been carefully handled to minimize the potential for ESD. In Fig. 2.7a, a thick (>50 nm) WO_x layer is seen to have formed on the specimen surface, which is inconsistent with normal growth expectations based on reactions of clean tungsten with air. In Fig. 2.7b, we see an example where a substantial region of oxide has formed at the end of the tip, consuming the previously FIB-targeted region of interest (ROI) in the specimen. Since most ESD events that result in tip morphology changes are not observable visually, good ESD tip handling protocols must be used. Continuous grounding of specimen holders and tweezers during transfer is common sense to help prevent ESD. When implemented, good practices can have a profound effect on the ability to manufacture and image APT specimens.

Some consideration must also be taken when shipping and transferring specimens. Non-ESD-compatible plastics can collect large amounts of static charge on the surface, which is difficult to dissipate and should be avoided. These charges may promote ESD by being transferred by non-grounded human touch to the specimen. Conducting specimen carrier covers and tweezers that are grounded during transfer provide the best protection. Conductive plastic carriers with anti-static plastic covers have also proven adequate to protect STM tips and APT microtip arrays during transport.

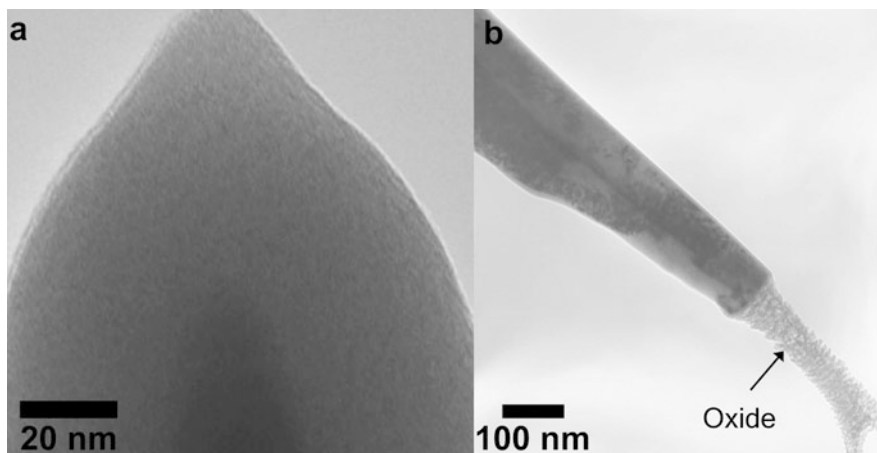


Fig. 2.7 Examples of ESD damage. (a) TEM image of a W tip that has been modified due to electrostatic discharge that results in the growth of WO_x . Regions of pure W (dark) and WO_x (light) are observed (reprinted with permission from Cambridge University Press [16]). (b) Substantial oxide grown on a ferritic alloy after site-specific specimen preparation had been performed (courtesy D. W. Saxey, University of Western Australia)

2.5 Focused Ion Beam Methods

Using ions to assist in the preparation of specimens for APT goes back nearly 40 years [19]. Broad ion beams have been used by a variety of researchers [20–25] to assist in specimen preparation, and early efforts were also made using FIB [26, 27], although the capability of these early instruments was not good enough for them to be broadly applied. The current generation of FIB instruments developed in the 1990s, however, has brought an entirely new capability to APT specimen preparation methodology. The combination of the capability to image specimens (using ions as the probe and secondary or backscattered electrons as the detected signal) with the capability to remove substantial amounts of material using ions provided something never before available: the ability to observe the features of interest in specimens at high magnification while they are being sharpened. Over the last decade or so, this capability has drastically modified the volume of applications to which APT may be successfully applied.

The earliest FIB-based methods used to sharpen specimens for APT relied on attaching a volume of material to the end of a needle [24, 28, 29] (using non-FIB methods) and shaping the end form for APT analysis with a FIB [14, 30–32]. Optimal annular milling methods were gradually developed that provided for improved tip shapes [12, 33–36]. These methods not only allow the user to see the majority of the specimen apex volume during preparation but are also generally applicable to almost all materials. If care is taken during the final steps of preparation, minimal

ion-induced damage will be present in the specimen ROI [37]. APT lift-out methods [36, 38–41] were adapted from transmission electron microscopy techniques [42]. These methods enabled removal of a small region of material, while being viewed in the FIB, *from nearly any starting structure*. This small region of material eventually forms the apex region of the specimen.

Today, many applications and variations of the standard lift-out and sharpening methods have been reported [36, 43–48]. These include variations enabling analysis parallel to the original specimen surface (cross-section orientation) [49] or inverted relative to the original specimen surface (backside orientation) [50, 51]. Details of these methods are described below.

2.5.1 Capping Considerations and Damage

In the context of APT, capping refers to the application of a sacrificial layer of material to the original surface of a sample. The primary purpose of this procedure is to protect the specimen from the gallium ions used during the lift-out process and subsequent sharpening, but there are a number of secondary considerations as well. These include (1) adequate adhesion of the capping layer to the specimen surface; (2) material properties which enhance control of the specimen manufacturing process (i.e., grain size, relative sputtering rate, imaging contrast); (3) potential mass spectrum peak interferences; and (4) and evaporation field requirements. Each of these is discussed below.

An illustration of the gallium ion implantation due to FIB milling is shown in Fig. 2.8. Here, a doped silicon wafer has been prepared using standard lift-out methods and annular milling techniques (described below). The final milling stage was performed on separate specimens using 30 and 5 keV gallium ions to investigate gallium ion implantation effects. Figure 2.8a shows an atom map from a specimen shaped with 5 keV gallium ions. As the analysis proceeds, the gallium implantation is greatly reduced as the analysis becomes farther removed from the original specimen surface. Figure 2.8b compares the penetration depth of 30 and 5 keV ions (as analyzed in the LEAP). The implantation region is reduced to ~5–10 nm for the 5 keV case. When using 2 keV ions for the final preparation stage, almost no residual gallium ions remain [37, 39]. Figure 2.8c shows a thermal scale representation (20 % gallium is shown in red) of the gallium implantation into SiN following a 5 keV final milling step. Note that this specimen was capped a second time immediately following the FIB sharpening step in order to bury the final milled surface for APT analysis. For comparison, simulations of gallium ion implantation into silicon [52] using either 30 or 5 keV ions are shown in Fig. 2.9a, b, respectively. Figure 2.9c quantifies the simulated implantation and suggests that, at least for FIB milling of silicon, one should always plan to remove ~20 nm of material prior to analyzing an undamaged ROI.

APT is a destructive technique (material is removed as the analysis proceeds), and so damaged regions of the specimen can be removed prior to data collection

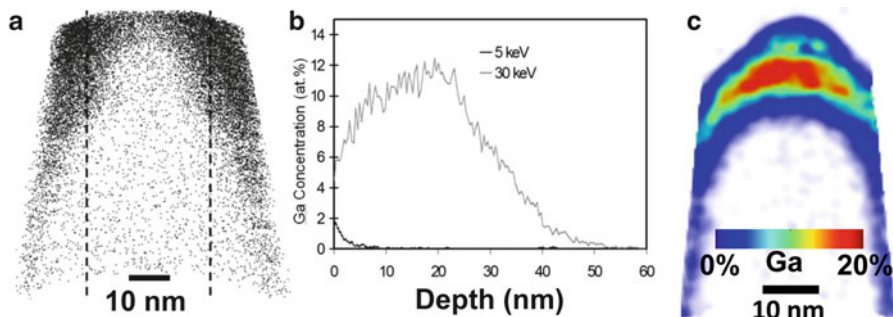


Fig. 2.8 Typical gallium implantation caused by FIB milling at 5 and 30 keV. (a) Atom map obtained from APT of a 5 keV-shaped silicon specimen. The *dark dots* represent individual gallium atoms. The *dashed lines* represent the analysis volume used to produce the atomic gallium composition as a function of depth shown in (b) (reprinted with permission from Elsevier [39]). (b) A comparison of the gallium composition profile with depth for a specimen shaped with 5 and 30 keV gallium ions (reprinted with permission from Elsevier [39]). (c) Gallium implantation into SiN following a 5 keV final milling step

and only undamaged volumes are typically retained for analysis. It is important to minimize gallium implantation as much as possible as damage may lead to intermixing of phases and regions of different compositions or even turn crystalline regions amorphous [30, 31, 36]. The damage may also promote the creation of regions with decreased structural integrity, increasing the chances that a specimen will fail prematurely under application of high electric field. In either case, minimizing gallium damage in a finished APT specimen is desirable.

For specimens where the original surface material is part of the ROI, it is desirable to retain some of the capping material in the final specimen shape for analysis to ensure damage-free analysis volumes and a buried interface. This requires a cap with strong interfacial adhesion to the native surface [53]. For microelectronics applications where silicon is the native surface material, common seed layer materials (which naturally have good adhesion) are good sources as a protective cap and include nickel, chromium, titanium, and silicon. Other criteria should be considered as well and are discussed below, but if the specimen cap/surface interface does not survive application of high electric field, then other considerations are moot.

Controlled ion milling properties are important for controlling the shape of the specimen/optic. Both the grain size and relative ion sputtering rates affect the tip shaping process. Ideally, a capping material possesses a very large grain size (or is amorphous) so that differential ion milling rates at grain boundaries do not induce undesired topography into the forming specimen. Extremely fine grains (much smaller than the tip dimension) produce a similar effect. Capping materials with sputtering rates similar to or lower than those of the specimen are also desirable.

Evaporation field [54] is another consideration. Evaporation field differences between layers are known to cause spatial reconstruction aberrations at interfacial regions [55, 56]. Considering a microelectronics application again, sputtered nickel

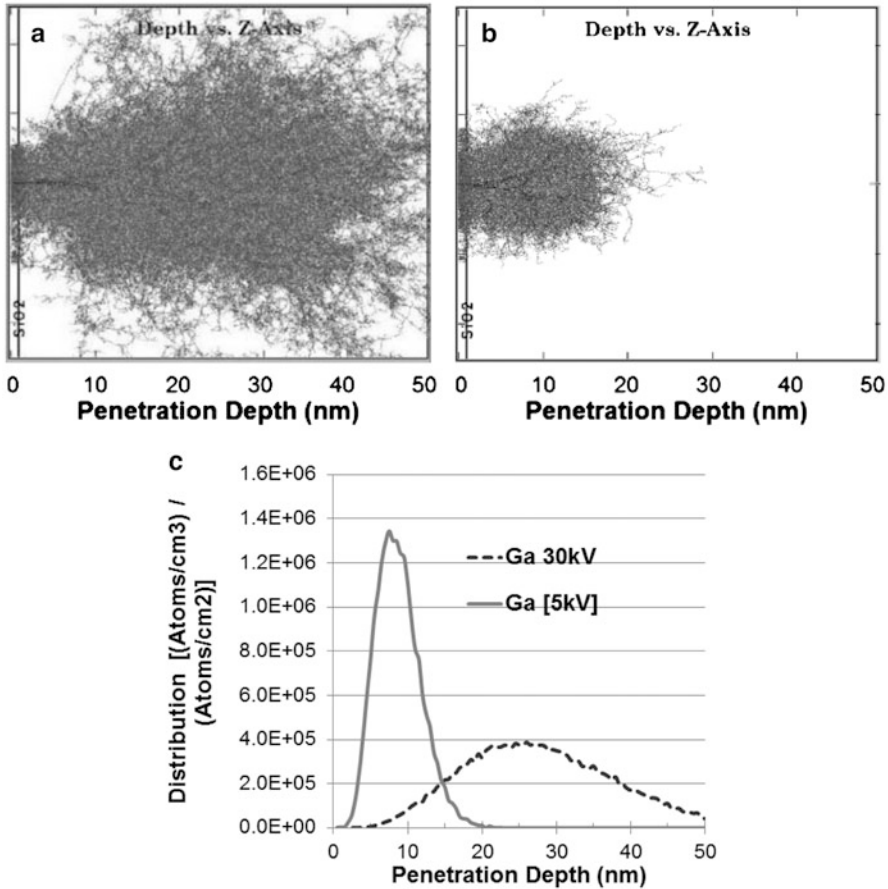


Fig. 2.9 SRIM [52] simulation of gallium ion implantation into silicon using (a) 30 keV and (b) 5 keV ions. (c) Concentration profile normal to the original silicon surface showing the implanted gallium ion depth

and polysilicon both have good adhesion and similar evaporation fields (less than ~10 % different) when compared to crystalline silicon and thus make reasonable choices as capping materials. However, the gallium ion stopping power of polysilicon is significantly less than that of nickel, and so a thicker cap of polysilicon would be necessary to provide equivalent protection.

Ion mass peak overlap is another capping consideration. In order to easily separate out the capping layer from the ROI, overlap of ion peaks from materials in adjacent layers should be avoided. Materials with a small number of isotopes that occupy unique regions of the mass spectrum are often considered for this reason alone. Unfortunately, they commonly suffer serious limitations when considered against the other capping considerations mentioned above. Gold has a single

isotope far separated from nearly any expected ROI mass peak but has poor adhesion and high sputtering yield compared to most materials. Cobalt likewise has a single isotope and is uniquely placed, especially with regard to other transition metals (no isotopic overlaps with iron or nickel), but it does not adhere particularly well to other materials. FIB-deposited materials such as tungsten and platinum (and even carbon) may adhere relatively well and have mass peaks that are often beyond the mass-to-charge range of most commonly analyzed materials, but they often contain high levels of carbon and gallium as a consequence of the carrier gas/ion deposition process [57] and have an extreme evaporation field, resulting in premature specimen failure.

Finally, very low deposition rates for a capping material can lead to undesirably long deposition times. For sputter-based deposition, it is the high sputtering yield that enables fast deposition, but during gallium milling, the same property limits tip shaping control as discussed earlier.

Multiple capping materials may also be used to manufacture a multilayer cap with a combination of desired properties [58, 59]. Again using the microelectronics example, a thin nickel or chromium layer may be selected for good adhesion to a crystal silicon surface, a layer of gold or platinum might be included for a highly visible end-point layer (with secondary electron imaging), gold or silver may be used because of the high deposition rate, and, finally, platinum has durability under ion milling (sputtering rate and gallium protection).

2.5.2 *Standard Lift-Out Process*

For material structures where (1) the ROI can be deduced from surface features, (2) the ROI resides near the surface, and (3) the analysis direction is intended to proceed from the top surface down into the material (typically referred to as top-down or normal orientation), the standard lift-out preparation is appropriate [36, 39, 40]. Although a number of variations of the general method exist [43–46, 48, 60–62], the specific steps illustrated below describe the method most commonly used by the current authors.

Figure 2.10 illustrates the general steps that the user should follow during a standard lift-out procedure. An optional protective capping layer may be applied over the entire specimen surface. No additional (i.e., non-FIB deposited) capping layer is used in the current example because the ROI is sufficiently far below the original surface of the sample. A FIB-deposited platinum strip is added to protect the surface and to mark the region to be extracted (arrowed in Fig. 2.10a). The platinum layer is typically 2–3 μm wide and ~ 100 nm thick with a length that depends on the geometry of the ROI and the number of desired specimens to be made from the extracted sample region.

Material is then removed around the specified ROI to create a wedge-shaped mass of material to be removed from the surface (Fig. 2.10b, arrows). In this case, trench 1 is created by tilting the stage to 22° (with respect to the electron beam) and

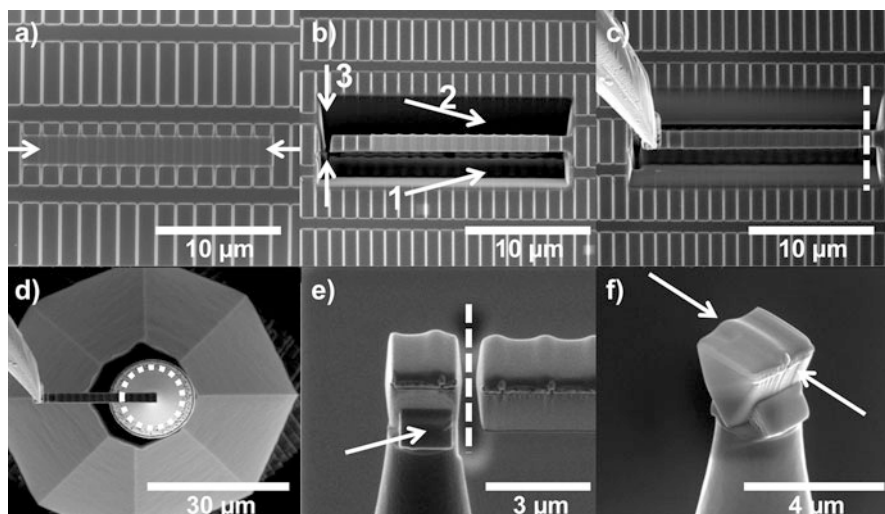


Fig. 2.10 The steps involved in a standard FIB lift-out procedure. (a) A FIB-deposited protective strip is placed over the region of interest. This protective material is often platinum or tungsten. (b) The material is then removed by ion milling around three sides of the region (*arrows*) as well as underneath to produce a long cantilevered wedge of material. (c) The wedge is removed by using an in situ micromanipulator (attached to the *left end* of the wedge) and then cutting the wedge free from the substrate (*dashed line*). (d) The micromanipulator is used to position the wedge above the carrier microtip (plan-view). (e) The wedge is attached to the carrier tip surface with FIB-deposited platinum (*arrow*) and then cut free from the carrier tip (*dashed line*) for transfer to additional microtips. Once propagation of the wedge is complete, the FIB stage is rotated 180° so that a second platinum deposition can be applied to the opposite wedge–post interface of each mounted post. (f) The final mounted wedge section is then ready for sharpening: The line of the targeted FinFET is clearly visible along the line of the *arrows* (reprinted with permission from Annual Reviews [77])

milling with a ~ 6 nA ion current in a ~ 2 μm -by- 10 μm rectangular pattern. The ion beam is scanned parallel to the long axis of the wedge starting far from the platinum strip and proceeding to the near edge. Trench 2 is created using the same procedure after rotating the stage through 180°. Milling is completed when trenches 1 and 2 meet beneath the ROI. Trench 3 is then cut using a ~ 1 – 2 μm long rectangular pattern of sufficient width to cut across the entire wedge leaving behind a cantilevered wedge. The 22° tilt coupled with these wedge and trench dimensions allows the user to observe the bottom of the trench in the SEM and better estimate the milling time required for complete undercutting of the wedge.

After returning the FIB stage to 0° tilt, a needle on a micromanipulator is lowered into contact with the free end of the cantilevered wedge (left edge of Fig. 2.10c). Sufficient FIB-deposited platinum is used to secure the micromanipulator to the top of the wedge. The cantilevered wedge is then cut free by milling a ~ 1 – 2 μm long rectangular pattern again (*dashed line*) with width sufficient to cut across the entire wedge.

Once the wedge and manipulator are lifted free of the bulk, the wedge can be repositioned above a carrier tip (Fig. 2.10d). In this image, the wedge is placed above a $\sim 2\ \mu\text{m}$ diameter, flat-topped, silicon microtip post (the post is centered within the dashed circle). The microtip posts are manufactured as a $450\ \mu\text{m}$ array with each post having an overall height of $\sim 100\ \mu\text{m}$ above a planar surface [13]. This height and spacing combination is sufficient to allow for rapid transfer of wedge material to multiple posts and to allow independent LEAP analysis of each post without field evaporating any neighboring specimens. The wedge is carefully lowered until it comes into direct contact with the flat surface on the top of the post. An $\sim 1\ \mu\text{m}$ -by- $1\ \mu\text{m}$ -by- $0.5\ \mu\text{m}$ platinum patch is deposited at the wedge–post interface to secure the wedge to the post (Fig. 2.10e, arrow). The region of the wedge secured to the post is then cut free, as indicated by the dashed line in Fig. 2.10e, and the wedge is moved to the next post and the procedure is repeated until the wedge is gone.

Once propagation of the wedge to the microposts is finished, the stage is rotated 180° so that a second platinum patch can be applied to the opposite side of the wedge–post interface for each mounted post. The final mounted wedge is shown in Fig. 2.10f, with the ROI located along the line indicated by the arrows. Subsequent cleaning of the micromanipulator to remove any remaining platinum or wedge material is recommended before reuse.

2.5.3 Sharpening Process

The required specimen dimensions for APT are material and instrument dependent, and the user must consider this fact, as well as the voltage-range limitation at which an atom probe can operate, when preparing specimens. If the user is planning to analyze materials that have particularly high evaporation fields ($\geq 40\ \text{V/nm}$), this should be taken into account when considering the final specimen radius. In addition, features of interest which are relatively large need to be positioned below the initial apex of a specimen. A general rule of thumb is to prepare a specimen which has a lateral diameter at the ROI depth position of about two times the lateral dimension of the ROI. Clearly this limits the size of features which may be totally contained in the field of view of a LEAP analysis.

The process of converting a lift-out wedge into a sub- $200\ \text{nm}$ diameter sharp needle is accomplished through a series of annular milling steps [31, 33] followed by a low-energy FIB cleanup step [37, 39], as shown in Fig. 2.11. Illustrated in Fig. 2.11a is a linear fin-shaped field-effect transistor (FinFET) structure centered within the wedge, shown by the arrow. Tip shaping is accomplished by applying an annular milling pattern (shown schematically at the top of Fig. 2.11b) with constant outer diameter ($\sim 4\ \mu\text{m}$) and a decreasing inner diameter (Fig. 2.11b–d) with a beam current of $\sim 0.28\ \text{nA}$. The milling proceeds from the outer diameter of the pattern to the inner diameter of the pattern to best control any potential for redeposition of removed material. The first pattern (Fig. 2.11b) has an inner diameter of $\sim 1.6\ \mu\text{m}$

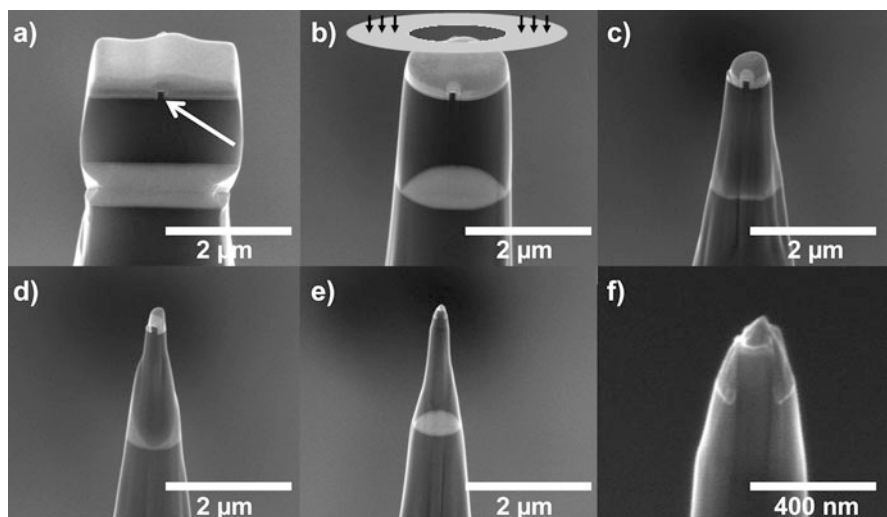


Fig. 2.11 The steps involved in FIB sharpening process converting the wedge section in Fig. 2.10 into a specimen for APT analysis. (a) The region of interest is shown by the *arrow*. (b) The first annular milling pattern shapes the tip into a cylinder, with the FinFET region clearly visible near the (c) upper-center portion of the cylinder. The second and third milling patterns produce (c) a tapered end and (d) a narrowed end. The final sharpening step is performed at low ion energy (either 2 or 5 keV) and is simply a circular pattern that images the specimen end-on. During this stage, the specimen is carefully monitored to ensure that the region of interest is positioned near the apex of the final specimen. The (e) low- and (f) high-magnification images of the specimen that is then ready for APT (reprinted with permission from Annual Reviews [77])

and produces a long cylindrical shape that proceeds well beyond the platinum-weld region of the wedge (not shown). The second and third patterns (Fig. 2.11c, d) have inner diameters of ~ 0.6 and ~ 0.3 μm , respectively. Each pattern is applied for a length of time sufficient to achieve the desired tip diameter to a location just beyond the length of the ROI. The final tip shaping is accomplished with the low-energy (5 keV) FIB cleanup step described below.

As mentioned previously, the implant and damage region created in silicon by a 30 keV gallium ion beam has been shown to extend significantly into the surface of the sample, while 2–5 keV ions limit damage to less than ~ 5 nm [37]. The goal of the low-energy (2–5 keV) milling step is to remove the 30 keV damaged region, position the apex of the specimen at or slightly above the ROI, and narrow the bottom section of the ROI to 200 nm or less in width. An annular milling pattern of >4 μm diameter is centered over the tip, and milling proceeds at a reduced beam current (48 pA in the current example). The diameter of the pattern and beam current can be adjusted to slow the rate of milling so that the user is able to carefully control the stopping point. Most current FIB instruments provide live viewing of ion milling which assists in real-time end-point control. After the final step, the specimen shape is shown in Fig. 2.11e, f. The total milling time for the final low ion

energy step is of the order of 60 s. Small variations in total milling time can quickly change the dimensions of the final tip shape. For example, an additional 5–10 s of milling in this case would move the tip apex position below the ROI.

2.5.4 FIB Deprocessing

In the preceding sharpening example, the necessary removal of a large amount of material (~500 nm) to reach the ROI may inhibit the capability to make a repeatable tip shape because of the influence of differential sputtering due to interaction with grain boundaries and/or multiple material regions. It is therefore desirable to control the amount of material above the ROI before initiating the tip-shaping procedure. Minimizing the capping material thickness is helpful in this regard, but full control of the distance between the ROI and the original surface is desirable. Likewise, a problematic region (e.g., an interface between two phases or a region of highly different evaporation field) may exist near the ROI such that removing that region from the tip apex with the low-energy cleanup step does not result in an appropriate final shape. In this case, complete or partial removal of the problematic region prior to FIB processing and the addition of a new sacrificial capping layer can enable proper shaping of the ROI volume.

Both of the above objectives can be accomplished via FIB deprocessing [61]. This process involves removing layers of material parallel to the original sample surface using FIB ion beam milling in a fashion very similar to TEM lamella production techniques [63]. An extracted wedge of material, like that in Fig. 2.10, is first rotated by 90° along its long axis enabling milling parallel to the original wedge surface. This rotation is usually accomplished by transferring the wedge to a manipulator that has an axial rotation capability [49]. Similar to final tip shaping, the SEM is used to control the end-point for the milling while performing FIB deprocessing.

Figure 2.12a shows a highly magnified image of a transistor exposed at the edge of an extracted wedge that has been rotated by 90°, with the exposed edge of the wedge shown at lower magnification in Fig. 2.12b. Approximately 500 nm of material must be removed to locate the top surface of the wedge near the gate oxide in this particular example. The user can carefully trim any amount of material from the surface. Figure 2.12c shows the stopping point one would choose if the top of the silicide region was the goal of the deprocessing, while Fig. 2.12d shows the stopping point just above the gate oxide in the transistors.

2.5.5 Cross-Section Preparation

Performing analysis along directions other than from the top surface into the bulk of the sample can have advantages. For example, analyzing thin films parallel to the film interface orientation (termed cross-section orientation) serves to both increase

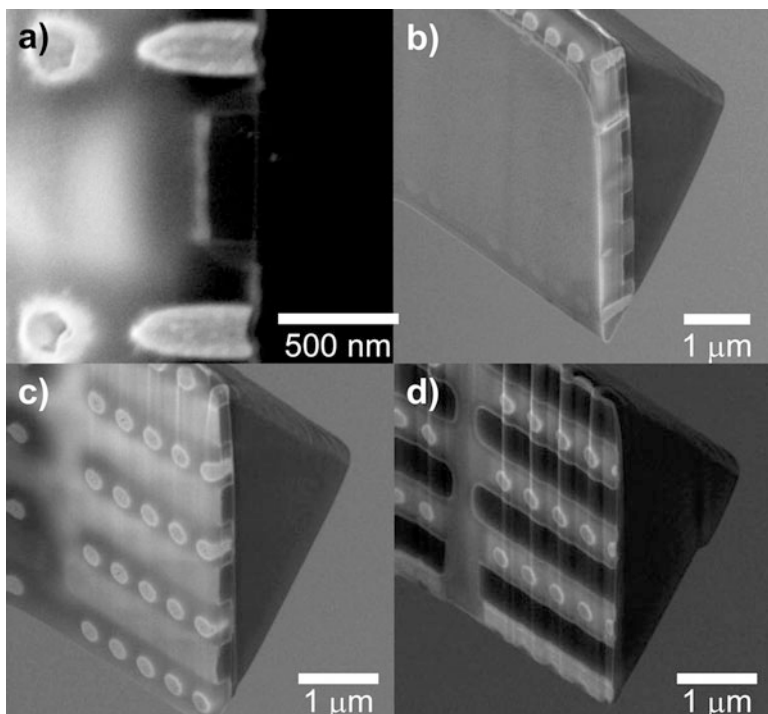


Fig. 2.12 An example of FIB deprocessing. (a) A rotated image of a transistor region within the wedge. (b) The original extracted wedge after it has been transferred to a manipulator that has been rotated by 90° . (c) Specimen wedge after it has been deprocessed to a point near the silicide region above the transistor. (d) Specimen wedge after it has been further deprocessed to a point just above the gate oxide region (reprinted with permission from World Scientific Publishing [60])

the volume of the ROI (the film interfaces) and improve the analysis yield by changing the orientation of the applied stress relative to the interface(s) (see Chap. 4 for a description of the stresses applied to an APT specimen). Figure 2.13 illustrates a cross-section specimen preparation procedure where the ROI consists of layers of material positioned at the original sample surface.

In such cases, as mentioned previously, a thick sacrificial cap is first added to the surface of the sample to protect the ROI and add additional material to the sample so that the surface or the near-surface ROI can be centered in the final tip [49]. In this case, ~ 500 nm of nickel has been deposited on the top surface of the sample before a standard lift-out procedure is used to create a large lift-out wedge (~ 5 μm wide).

After attaching the manipulator needle and extracting the wedge from the bulk sample, the wedge is transferred to a horizontal manipulator with a rotational degree of freedom (Fig. 2.13a). The wedge is transferred by first attaching it to the second manipulator with FIB-deposited platinum and then cutting the original manipulator from the wedge. While attached to the horizontal manipulator, one side

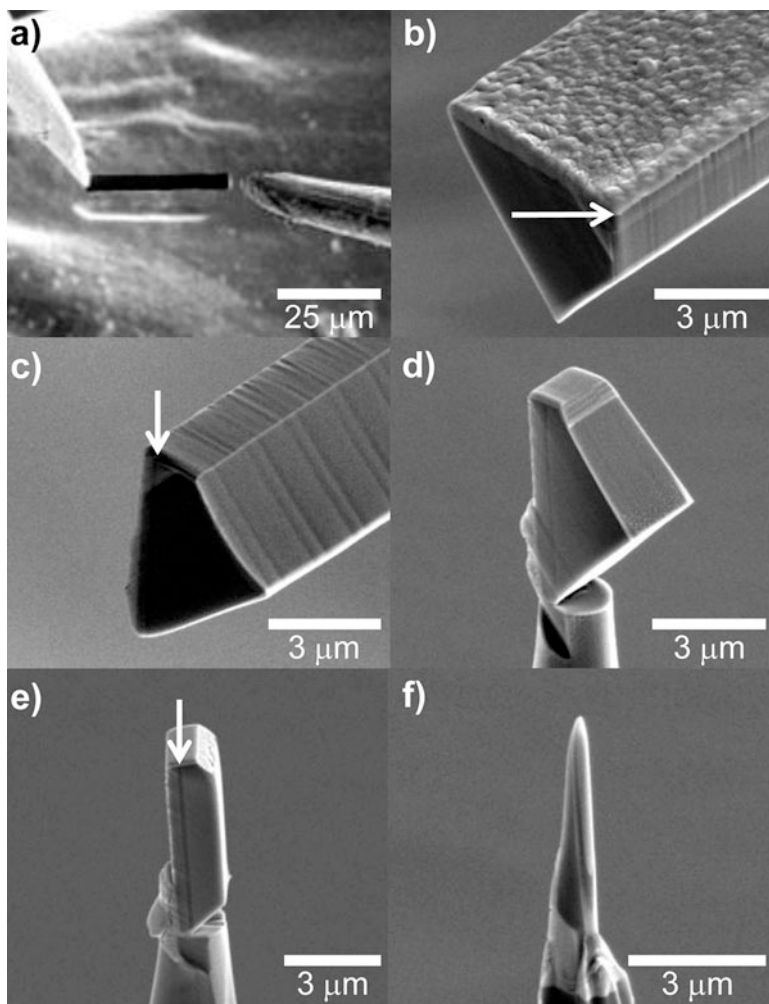


Fig. 2.13 The steps for performing site-specific lift-out and manipulation for cross-section APT specimens. (a) The original capped specimen wedge is transferred to a manipulation probe which allows rotation of the wedge. (b) Original wedge still in normal orientation is FIB cut to expose cross-section ROI (see *arrow*) (c) Wedge is rotated by 90°, and the cross-section ROI surface is capped ready for final preparation (ROI indicated by *arrow*). (d) A wedge section is mounted to a post. (e) The mount is trimmed prior to annular milling. (f) The final tip with cross-section ROI captured at the tip (reprinted with permission from World Scientific Publishing [60])

of the wedge is milled flat, creating a new surface that is at 90° to the original surface, as shown in Fig. 2.13b (this will become the top surface of the final tip). The arrow highlights a dark layer below the 500 nm nickel cap which is the location of the ROI for this example. For site-specific cross-section preparation, this new surface also needs to be positioned directly adjacent to (above in the final tip) the feature of interest.

After this new surface is created, the wedge is rotated back by 90° and an additional capping layer (~50 nm nickel) is added to the new surface, Fig. 2.13c. Sufficient capping material on the new surface ensures that the specimen can be shaped with 30 kV ions and finished with 5 kV ions without exposing any of the original sample material to gallium ions. Should this second cap be removed before final specimen preparation is complete, differential milling of the different layers can cause the tip to form into multiple protrusions.

Once the second capping material has been deposited, the wedge is transferred back to the original micromanipulator and propagated to microtips in a manner similar to the standard lift-out method described above (Fig. 2.10). Figure 2.13d shows a portion of the wedge after it has been successfully propagated to a carrier tip. Before tip shaping can begin, an effort is made to make the tip more cylindrical. The portion of the wedge that extended beyond the edge of the microtip is removed with a rectangular milling pattern before sharpening (Fig. 2.13e). The final specimen shape after the standard annular milling and low-energy cleanup steps described above is shown in Fig. 2.13f.

The standard annular milling process is not quite as straightforward for cross-section preparation because the ion milling rate of the specimen is likely to have non-cylindrical symmetry. Any differential ion sputtering between layers will cause asymmetry in the final shape. Often the center of the milling pattern will need to be positioned away from the center of the region in anticipation of one side of the specimen milling at a higher rate. The proper amount of this pattern shift is usually determined by trial and error. A capping material used on the original surface chosen to have similar milling properties of the ROI will assist in the mitigation of this phenomenon.

2.5.6 Backside Preparation

Analyzing materials starting from within the bulk and proceeding toward the original sample surface (termed backside) [50, 51] can serve multiple purposes. Should weak or otherwise problematic materials or interfaces exist between the sample surface and the ROI, analysis from the backside may allow for these regions to be avoided. If there is a substantial thickness of insulating material (thermal or electrical) present beneath the ROI, backside preparation may also prove useful, as this material can be removed from the final specimen. In addition, specimen shape distortions, and the resultant effects on data reconstruction, can be affected by the order of evaporation of regions with different evaporation fields. Performing analysis both in the top-down and backside orientations can provide meaningful information to help separate real compositional trends from artifacts [64, 65].

Depending on the location of the ROI, backside specimen preparation may require application of significant material to the top surface of the sample so that the overall depth of the wedge remains ~2–3 μm after it has been rotated 180° and formed into a sharp specimen. As in previous examples, adhesion of the added material to the original sample surface is very important because that interface will

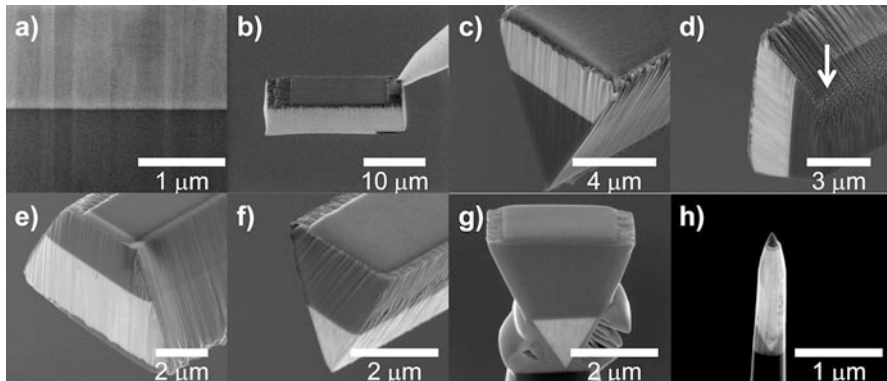


Fig. 2.14 An example of backside specimen preparation. The target ROI is the near-surface region of a primarily silicon material. An $\sim 2\ \mu\text{m}$ layer of sacrificial material (silver) has been added to bury the original surface. (a) The FIB is used to cut a trench into this composite material to expose the original surface within the depth of the sample. The interface is observed $\sim 2\ \mu\text{m}$ below the surface. (b, c) A larger-than-normal wedge is extracted from the host material with a micromanipulator. (d) After transfer to a second micromanipulator with a rotational degree of freedom, the wedge is rotated by 90° and the material is removed to expose the new uppermost surface (arrow). (e) The wedge is rotated another 90° so that the uppermost surface is properly oriented. (f) The wedge is reshaped so that the former top part of the original wedge has a triangular shape to enable attachment via FIB-deposited platinum. (g) An image of the upside-down, reshaped wedge after attachment to a microtip post using FIB-deposited platinum. (h) Final tip shape after all annular milling steps have been completed

reside near the apex of the final specimen. One successful recipe used a palladium seed layer followed by a silver layer $\sim 3\ \mu\text{m}$ thick to provide the necessary thickness for the backside procedure [51, 65]. The palladium provides good adhesion to the top metallic surface and to the silver [66], while the use of silver as a capping layer allows for very fast deposition of the $3\ \mu\text{m}$ of material and good electrical and thermal conduction. The actual steps of the backside specimen preparation procedure are similar to those for a cross-section specimen.

Figure 2.14 illustrates the backside specimen preparation process for a ROI that resides near the sample surface. First the top surface is sufficiently buried ($\sim 2\ \mu\text{m}$ silver with a palladium seed). Then, a trench is cut into the surface of the sample to expose the depth of the material for SEM imaging. The buried interface is clearly visible in Fig. 2.14a, confirming that the target ROI resides some $2\ \mu\text{m}$ below the surface. Similar to cross-section specimen preparation, a larger-than-normal wedge ($\sim 5\ \mu\text{m}$ wide) of material is extracted and transferred to a micromanipulator with a rotational degree of freedom (Fig. 2.14b, c). The goal of the next set of steps is to place the ROI near the top of a new wedge with triangular cross section. To accomplish this, the wedge (Fig. 2.14c) is rotated 90° and material is removed (arrow in Fig. 2.14d) with the FIB so that the ROI is near the new surface. Then, the wedge is rotated another 90° so that the original wedge is upside down (Fig. 2.14e). At this point an optional second capping layer may be added to the newly created top surface to protect it during the annular milling process.

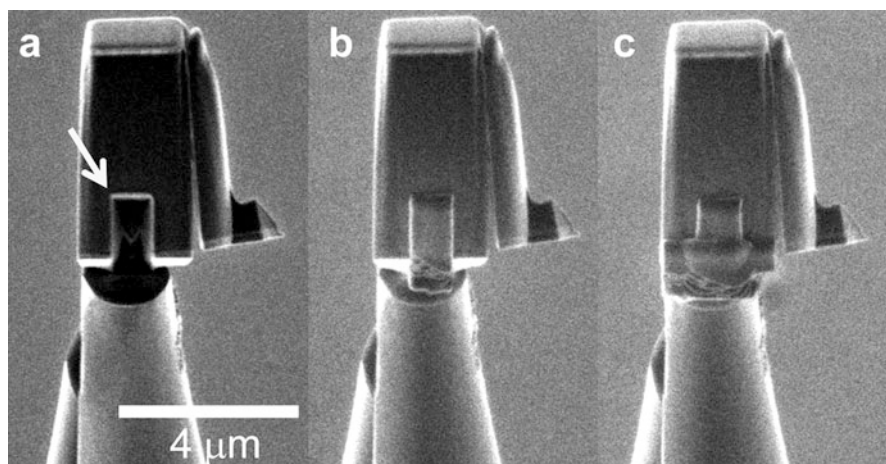


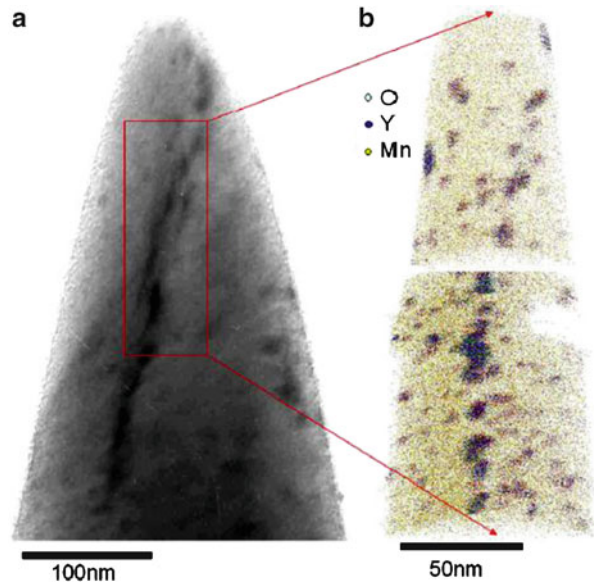
Fig. 2.15 An example of the mortis and tenon method for wedge attachment to a carrier post. (a) First a keyhole is milled through the object that is being attached to the carrier post (*arrow*). This is commonly performed while the wedge is still attached to the micromanipulator (not illustrated here). (b) Next the keyhole is filled with FIB-deposited platinum using a pattern of the same size used in the milling step. (c) Because this wedge surface is oriented 90° to the carrier surface, it is possible to make an additional FIB-deposited platinum weld to confidently secure the lift-out to the carrier. Other wedge surface/carrier orientations may only allow for attachment through the keyhole

To complete the wedge-shaping process, the stage is tilted to 22° with respect to the electron column and each side of the wedge is trimmed until the triangular cross section is formed (Fig. 2.14f). This shaping is necessary so that the FIB-deposited platinum can access the intersection of the wedge and carrier tip with zero stage tilt. Alternative adhesion strategies, such as the notch or mortise and tenon weld (see Fig. 2.15) [40], can be used which do not require a triangular wedge cross section to enable FIB adhesion. Finally, the wedge is transferred back to the mounting micromanipulator, and the wedge material is transferred to carrier posts (Fig. 2.14g) and annularly milled to its final tip shape (Fig. 2.14h).

2.6 Hybrid Transmission Electron Microscopy/Atom Probe Tomography

Transmission electron microscopy (TEM) and APT each has different advantages and limitations, but together they provide complementary information enabling more complete characterization of the microstructure and chemistry of a materials system. Although FIB/SEM images provide some information about the structure of an APT specimen after the specimen fabrication process, higher resolution

Fig. 2.16 TEM and APT analysis performed on the same specimen volume. (a) Bright field TEM image of an APT specimen prior to analysis showing a grain boundary within the analysis volume. (b) 3D reconstruction of the APT data obtained from the same tip with oxide particles present both along the grain boundary and in the bulk material (reprinted with permission from Elsevier [73])



characterization of specimens using TEM is useful to further increase APT reconstruction accuracy. TEM imaging can provide specimen radius and shank angle with high accuracy and also provide some information on the internal structure of interfaces and precipitates.

Analytical techniques such as energy-dispersive X-ray spectroscopy and electron energy loss spectroscopy, as well as different imaging modes in scanning TEM, can provide preliminary information about the composition of precipitates and interfaces. In addition, TEM can be used to obtain atomic resolution structural information that can be correlated with the compositional information obtained from APT.

A number of groups have reported progress in developing general hardware and methods that allow straightforward TEM and APT analysis of the same specimen [50, 51, 64, 67–74]. Although some physical limitations exist for specimen geometries and holders that are compatible with commercially available TEM and APT instruments, general wire-based and half-grid-based solutions do exist.

An example of results from TEM and APT of the same specimen is illustrated in Fig. 2.16 [73]. In this case, an oxide dispersion-strengthened (ODS) variation of the Eurofer 97 steel was fabricated and analyzed with high-resolution TEM followed by APT. Oxide particles measuring 5–10 nm in diameter were observed with TEM, but only APT could adequately characterize the local composition. As seen in the figure, particles appear aligned along planar features that could be lath or twin boundaries. Although large precipitates are obvious in the atom map, the smaller particles (~ 2 nm in diameter) are more uniformly distributed with a particle density of $3.9 \pm 0.15 \times 10^{23} \text{ m}^{-3}$ [73].

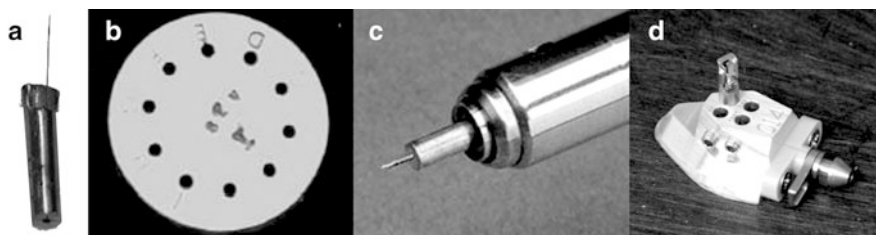


Fig. 2.17 Fixtures available to handle transfer of wire-shaped specimens. (a) Wire secured in a 1.8 mm copper sleeve. (b) SEM/FIB-compatible holder that can accommodate multiple 1.8 mm objects. (c) 1.8 mm copper sleeve mounted within a Fischione TEM holder. (d) APT holder that can accommodate multiple 1.8 mm objects

2.6.1 Preparation and Holders

Wire-shaped specimen geometries are common in APT and are very useful for TEM because the approximately cylindrical specimen cross section presents a constant sample thickness for all angles in a TEM tomography acquisition [75]. A wire itself may be difficult to handle and subsequently mount in a holder, so the wire can be secured in a thicker fixture such as the crimpable 1.8 mm copper sleeve shown in Fig. 2.17a. Wires are typically electropolished to a sharp tip so that they can be analyzed as-polished or taken into the FIB for further processing either as a specimen or a specimen carrier. Multiple wire specimens can be loaded into the FIB using a carrier similar to that shown in Fig. 2.17b. A set screw is used to secure Cu stubs into each hole of the holder. After FIB processing is complete, wires can be placed into appropriate holders for TEM analysis. For example, the Fischione (Export, PA, USA) 2050 TEM specimen holder and LEAP wire specimen puck are shown in Fig. 2.17c, d, respectively. These examples demonstrate how single-wire specimens can be successfully shared between FIB, TEM, and APT instruments with minimal difficulty.

Half-grid-shaped specimen geometries have become quite commonplace in TEM and can be accommodated in the LEAP as well. Advantages include a geometry where the specimen is protected by the superstructure of the grid, the fact that multiple tips may be carried on a single grid, and the common availability of TEM holders compatible with grids in non-APT laboratories. In Fig. 2.18, three different half-grid-format specimen carriers are shown: (a) a tungsten needle embedded via the Short-Cut™ into an Omniprobe® (Dallas, TX, USA) copper half-grid [51]; (b) a wire grid that has been cut in half and electropolished sufficiently sharp for analysis or mounting of lift-out specimens; and (c) a Dune Sciences' (Eugene, OR, USA) silicon half-grid with multiple specimen carrier regions that are compatible for mounting lift-out specimens. Examples of grid-compatible TEM holders and their LEAP-compatible specimen pucks are shown in Fig. 2.19. Figure 2.19a, top, shows a generic TEM grid holder and LEAP puck with

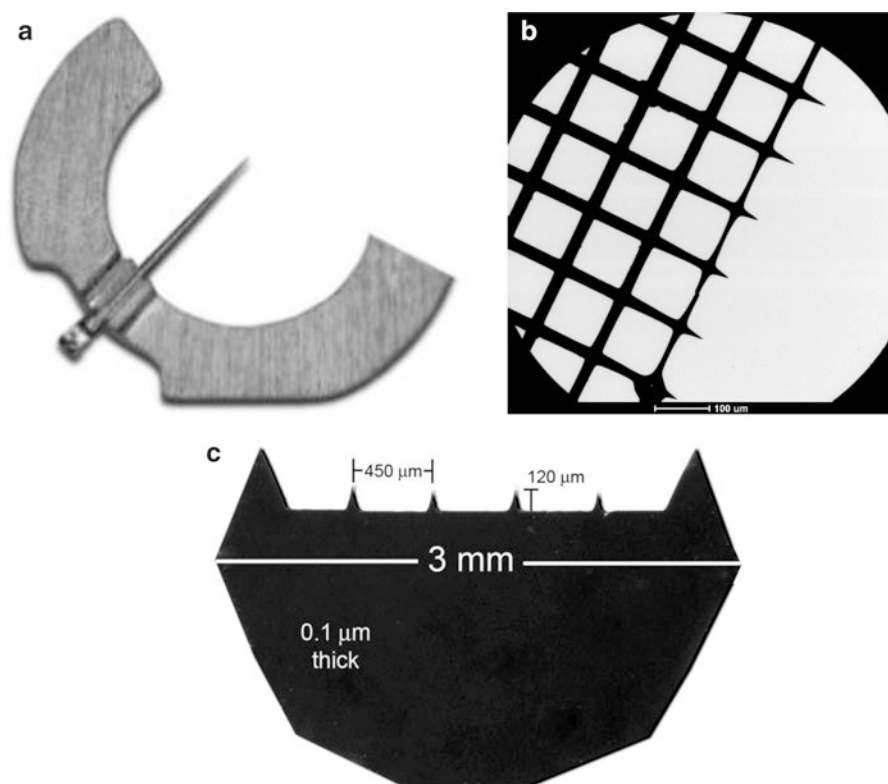


Fig. 2.18 Three half-grid-format specimen carrier options: (a) needle embedded via the Short-Cut™ into an Omniprobe copper half-grid, (b) a wire grid that has been cut in half and electropolished so that the ends are sharp, and (c) a Dune Sciences' silicon half-grid with multiple carriers (image courtesy of Dune Sciences', Eugene, OR, USA)

holder designed to hold a half-grid. The grid holder shown in the LEAP puck (Fig. 2.19b, top) serves double duty as a grid carrier for the LEAP, but it can also be carried into the FIB. With this approach, the user must handle the grid during some of the transfers between FIB, TEM, and LEAP instruments. The Hummingbird Scientific grid holder [50], Fig. 2.19a, bottom, consists of a removable end effector that can be placed in a TEM holder or a LEAP puck. The advantage is that once a half-grid is mounted in the end effector, it can be moved from FIB to transmission electron microscope to LEAP without the need for handling the grid directly with tweezers. Variations on the half-grid theme exist as well. Gorman et al. have used the Short-Cut to host a micromanipulator needle, which serves as a specimen carrier with the sharpened lift-out material at its apex [50]. Similar advances have been made recently by Felfer et al. [76].

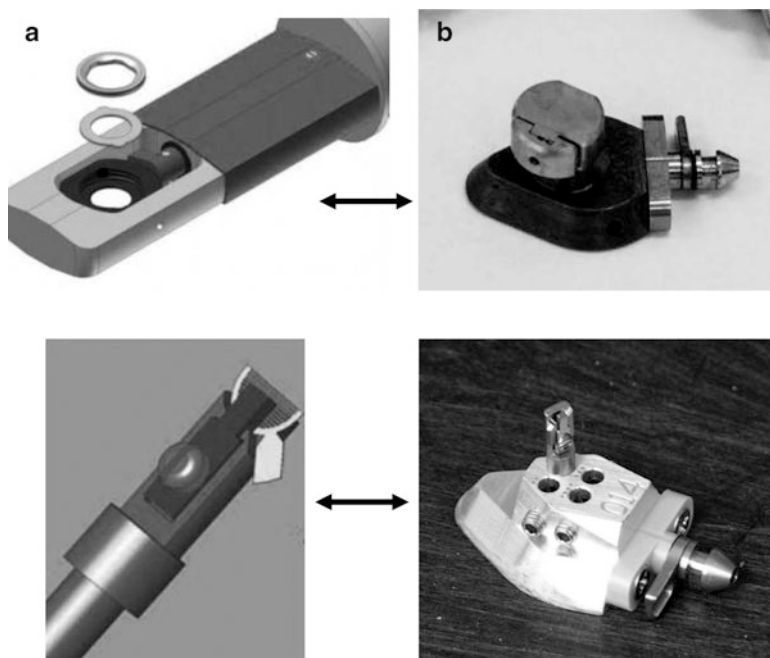


Fig. 2.19 TEM/APT specimen holder options. (a) TEM grid holders (*top* reprinted with permission from www.gatan.com; *bottom* reprinted with permission from Cambridge University Press [50]) and (b) their equivalent LEAP-compatible specimen carriers. A generic half-grid handling strategy is shown at the *top* of the figure, while the Hummingbird removable end effector strategy is shown at the *bottom* of the figure

2.7 Summary

Electropolishing and FIB-based specimen preparation methods give APT practitioners a number of options for manufacture of specimens from bulk materials. The technologically simple and inexpensive electropolishing method is still highly useful for metallurgical materials with a uniform distribution of features and an established polishing recipe. FIB-based methods have recently experienced rapid development and adoption because FIB instruments are now much more widely available and because of the compatibility of the lift-out technique with microtips. The capability of the local-electrode geometry to analyze microtips allows rapid, consistent, and controlled manufacture of multiple specimens in a short period of time. Further advantages include the ability to perform site-specific specimen preparation and FIB deprocessing, which are crucial capabilities for expanding the application space and success rate of APT experiments in general.

References

1. Müller, E.W.: Field Ion microscopy. *Science* **149**(3684), 591–601 (1965)
2. Thompson-Russell, K.C., Edington, J.W.: Electron Microscope Specimen Preparation Techniques in Materials Science. Monographs on Practical Electron Microscopy in Materials Science, vol. 5. Philips Technical Library, Eindhoven (1977)
3. Miller, M.K., Smith, G.D.W.: Atom Probe Microanalysis: Principles and Applications to Materials Problems. Materials Research Society, Pittsburgh, NJ (1989)
4. Miller, M.K., Cerezo, A., Hetherington, M.G., Smith, G.D.W.: Atom Probe Field Ion Microscopy. Oxford University Press, Oxford (1996)
5. Miller, M.K.: Atom Probe Tomography: Analysis at the Atomic Level. Kluwer Academic/Plenum Publishers, New York, NY (2000)
6. Tsong, T.T.: Atom-Probe Field Ion Microscopy: Field Ion Emission and Surfaces and Interfaces at Atomic Resolution. Cambridge University Press, Cambridge (1990)
7. Bowkett, K.M., Smith, D.A.: Field-Ion Microscopy. North-Holland, Amsterdam (1970)
8. Müller, E.W., Tsong, T.T.: Field Ion Microscopy Principles and Applications. Elsevier, New York, NY (1969)
9. Gault, B., Moody, M.P., Cairney, J.M., Ringer, S.P.: Atom Probe Microscopy. Springer series in materials science, vol. 160. Springer, New York, NY (2012)
10. Melmed, A.J.: The art and science and other aspects of making sharp tips. *J. Vac. Sci. Tech.* **B9**(2), 601–609 (1991)
11. Kostrna, S.L.P., Peterman, J.W., Prosa, T.J., Wiener, S.A., Larson, D.J., Kelly, T.F.: An automatic electropolishing system for needle-shaped specimens. *Microsc. Microanal.* **12**(S2), 1750–1751CD (2006)
12. Larson, D., Wissman, B.D., Martens, R., Viellieux, R.J., Kelly, T.F., Gribb, T.T., Erskine, H. F., Tabat, N.: Advances in atom probe specimen fabrication from planar multilayer thin film structures. *Microsc. Microanal.* **7**, 24–31 (2001)
13. Thompson, K., Larson, D.J., Ulfing, R.: Pre-sharpened and flat-top microtip coupons: a quantitative comparison for atom-probe analysis studies. *Microsc. Microanal.* **11**(S2), 882 (2005)
14. Larson, D.J., Petford-Long, A.K., Cerezo, A., Smith, G.D.W., Foord, D.T., Anthony, T.C.: Three-dimensional atom probe field-ion microscopy observation of Cu/Co multilayer film structures. *Appl. Phys. Lett.* **73**(8), 1125–1127 (1998)
15. Kaiser, K.L.: Electrostatic Discharge. CRC Press, New York, NY (2005)
16. Gorman, B.P., Ballard, J., Romanes, M., Jager, D., Reidy, R.F., Randall, J.N.: Mediation of electrostatic discharge induced morphological damage in atomically precise tips. *Microsc. Microanal.* **16**(S2), 480–481 (2010)
17. Andrén, H.-O., Henjered, A., Nordén, H.: Field corrosion of field-ion microscope specimens caused by polymer gaskets. *J. Phys. E Sci. Instrum.* **13**, 392–395 (1980)
18. Saxey, D.W.: Personal Communication (2011)
19. Walls, J.M., Southworth, H.N., Rushton, G.J.: The preparation of field electron/field ion emitters by ion etching. *Vacuum* **24**(10), 475–479 (1974). doi:[10.1016/0042-207x\(74\)90009-8](https://doi.org/10.1016/0042-207x(74)90009-8)
20. Henjered, A., Norden, H.: A controlled specimen preparation technique for interface studies with atom-probe field-ion microscopy. *J. Phys. E Sci. Instrum.* **16**(7), 617–619 (1983). doi:[10.1088/0022-3735/16/7/014](https://doi.org/10.1088/0022-3735/16/7/014)
21. Hellsing, M.: High-resolution microanalysis of binder phase in as sintered WC-Co cemented carbides. *Mater. Sci. Technol.* **4**(9), 824–829 (1988)
22. Kvist, A., Andren, H.-O., Lundin, L.: A specimen preparation technique for atom probe analysis of the near-surface region of cemented carbides. *Appl. Surf. Sci.* **94/95**(1–4), 356–361 (1996)
23. Larson, D.J., Camus, P.P., Vargas, J.L., Kelly, T.F., Miller, M.K.: Specimen preparation and atom probe field ion microscopy of BSCCO-2212 superconductors. *J. Phys.* **6**(C5), 271–276 (1996)

24. Larson, D.J., Petford-Long, A.K., Cerezo, A.: Field ion microscopy of multilayer film devices. *Microsc. Microanal.* **4**(S2), 112–113 (1998)
25. Larson, D.J., Russel, K., Cerezo, A.: Sharpening of field-ion specimens and positioning of features of interest by ion-beam milling. *J. Vac. Sci. Tech.* **18**(1), 328–333 (2000)
26. Waugh, A.R., Payne, S., Worrall, G.M., Smith, G.D.W.: In situ ion milling of field ion specimens using a liquid metal ion source. *J. Phys.* **45**(C9), 207–209 (1984)
27. Alexander, K.B., Angelini, P., Miller, M.K.: Precision ion milling of field-ion specimens. *J. Phys. Colloq.* **50**(C8), 549–554 (1989)
28. Hasegawa, N., Hono, K., Okano, R., Fujimori, H., Sakurai, T.: A method for preparing atom probe specimens for nanoscale compositional analysis of metallic thin films. *Appl. Surf. Sci.* **67**(1–4), 407–412 (1993)
29. Martens, R.L., Larson, D.J., Kelly, T.F., Cerezo, A., Clifton, P.H., Tabat, N.: Preparation of three-dimensional atom probe samples containing multilayer thin film structures using a focused ion-beam. *Microsc. Microanal.* **6**, 522–523 (2000)
30. Larson, D.J., Foord, D.T., Petford-Long, A.K., Cerezo, A., Smith, G.D.W.: Focused ion-beam specimen preparation for atom probe field-ion microscopy characterization of multilayer film structures. *Nanotechnology* **10**, 45–50 (1999)
31. Larson, D.J., Foord, D.T., Petford-Long, A.K., Anthony, T.C., Rozdilsky, I.M., Cerezo, A., Smith, G.D.W.: Focused ion-beam milling for field-ion specimen preparation: preliminary investigations. *Ultramicroscopy* **75**, 147–159 (1998)
32. Larson, D.J., Petford-Long, A.K., Cerezo, A., Smith, G.D.W.: Three-dimensional atom probe studies of metallic multilayers. *Acta Mater.* **47**(15), 4019–4024 (1999)
33. Larson, D.J., Foord, D.T., Petford-Long, A.K., Liew, H., Blamire, M.G., Cerezo, A., Smith, G.D.W.: Field-ion specimen preparation using focused ion-beam milling. *Ultramicroscopy* **79**, 287–293 (1999)
34. Larson, D.J., Petford-Long, A.K., Ma, Y.Q., Cerezo, A.: Information storage materials: nanoscale characterization by three-dimensional atom probe analysis. *Acta Mater.* **52**(10), 2847–2862 (2004)
35. Miller, M.K.: Sculpting needle-shaped atom probe specimens with a dual beam FIB. *Microsc. Microanal.* **11**(S2), 808 (2005)
36. Miller, M.K., Russell, K.F., Thompson, G.B.: Strategies for fabricating atom probe specimens with a dual beam FIB. *Ultramicroscopy* **102**, 287–298 (2005)
37. Thompson, K., Gorman, B.P., Larson, D.J., van Leer, B., Hong, L.: Minimization of Ga induced FIB damage using low energy clean-up. *Microsc. Microanal.* **12**(S2), 1736CD (2006)
38. Kelly, T.F., Martens, R.L., Goodman, S.L.: Methods of sampling specimens for microanalysis. United States Patent 6,576,900, June 10, 2003
39. Thompson, K., Lawrence, D.J., Larson, D.J., Olson, J.D., Kelly, T.F., Gorman, B.: In-situ site-specific specimen preparation for atom probe tomography. *Ultramicroscopy* **107**, 131–139 (2007)
40. Miller, M.K., Russell, K.F., Thompson, K., Alvis, R., Larson, D.J.: Review of atom probe fib-based specimen preparation methods. *Microsc. Microanal.* **13**, 428–436 (2007)
41. Miller, M.K., Russell, K.F.: Atom probe specimen preparation with a dual beam SEM/FIB miller. *Ultramicroscopy* **107**(9), 761–766 (2007)
42. Giannuzzi, L.A., Drown, J.I., Brown, S.R., Irwin, R.B., Stevie, F.A.: Focused ion beam milling and micromanipulation lift-out for site specific cross-section TEM specimen preparation. *Mater. Res. Soc. Symp. Proc.* **480**, 19–27 (1997)
43. Cairney, J.M., Saxey, D.W., McGrouther, D., Ringer, S.P.: Site-specific specimen preparation for atom probe tomography of grain boundaries. *Phys. B Condens. Mater.* **394**, 267–269 (2007)
44. Takahashi, J., Kawakami, K., Yamaguchi, Y., Sugiyama, M.: Development of atom probe specimen preparation techniques for specific regions in steel materials. *Ultramicroscopy* **107**(9), 744–749 (2007)
45. Saxey, D.W., Cairney, J.M., McGrouther, D., Honma, T., Ringer, S.P.: Atom probe specimen fabrication methods using a dual FIB/SEM. *Ultramicroscopy* **107**(9), 756–760 (2007)

46. Perez-Willard, F., Wolde-Giorgis, D., Al Kassab, T., Lopez, G.A., Mittemeijer, E.J., Kirchheim, R., Gerthsen, D.: Focused ion beam preparation of atom probe specimens containing a single crystallographically well-defined grain boundary. *Micron* **39**, 45–52 (2008)
47. Rachbauer, R., Massl, S., Stergar, E., Felfer, P., Mayrhofer, P.H.: Atom probe specimen preparation and 3D interfacial study of Ti-Al-N thin films. *Surf. Coat. Tech.* **204**(11), 1811–1816 (2010). doi:[10.1016/j.surfcoat.2009.11.020](https://doi.org/10.1016/j.surfcoat.2009.11.020)
48. Felfer, P., Ringer, S.P., Cairney, J.M.: Shaping the lens of the atom probe: fabrication of site specific, oriented specimens and application to grain boundary analysis. *Ultramicroscopy* **111**(6), 435–439 (2011)
49. Lawrence, D., Alvis, R., Olson, D.: Specimen preparation for cross section atom probe analysis. *Microsc. Microanal.* **14**(S2), 1004–1005 (2008)
50. Gorman, B.P., Diercks, D., Salmon, N., Stach, E., Amador, G., Hartfield, C.: Hardware and techniques for cross-correlative TEM and atom probe analysis. *Microsc. Today* **16**(4), 42–47 (2008)
51. Prosa, T.J., Lawrence, D., Olson, D., Larson, D.J., Marquis, E.A.: Backside lift-out specimen preparation: reversing the analysis direction in atom probe tomography. *Microsc. Microanal.* **15**(S2), 298–299 (2009)
52. Ziegler, J.: The stopping and range of ions in matter. <http://www.srim.org/> (2011).
53. Ohring, M.: *The Materials Science of Thin Films*. Academic, New York, NY (1992)
54. Tsong, T.T.: Field ion image formation. *Surf. Sci.* **70**, 211–233 (1978)
55. Vurpillot, F., Cerezo, A., Blavette, D., Larson, D.J.: Modeling image distortions in 3DAP. *Microsc. Microanal.* **10**, 384–390 (2004)
56. Larson, D.J., Geiser, B.P., Prosa, T.J., Gerstl, S.S.A., Reinhard, D.A., Kelly, T.F.: Improvements in planar feature reconstructions in atom probe tomography. *J. Microsc.* **243**, 15 (2011)
57. Gerstl, S.S.A., Morrone, A., Kvitek, R.: Three-dimensional nanoscale characterization of Pt deposition from an organometallic precursor induced by a focused ion beam. *Microsc. Microanal.* **12**(S2), 1252–1253 (2006)
58. Mutas, S., Klein, C., Gerstl, S.S.A.: Investigation of the analysis parameters and background subtraction for high-k materials with atom probe tomography. *Ultramicroscopy* **111**, 546–551 (2011)
59. Francois-Saint-Cyr, H.G., Mutas, S., Prosa, T.J., Ulfig, R.M., Klein, C., Lawrence, D., Olson, D., Larson, D.J.: Assessment of protective coatings used in focused-ion-beam specimen preparation for atom probe tomography. Abstracts of 53rd International Field Emission Symposium, 216 (2012)
60. Larson, D.J., Prosa, T.J., Lawrence, D., Geiser, B.P., Jones, C.M., Kelly, T.F.: Atom probe tomography for microelectronics. In: Haight, R., Ross, F., Hannon, J. (eds.) *Handbook of Instrumentation and Techniques for Semiconductor Nanostructure Characterization*, vol. 2, pp. 407–477. World Scientific Publishing, London (2011)
61. Larson, D.J., Lawrence, D., Olson, D., Prosa, T.J., Ulfig, R.M., Reinhard, D.A., Clifton, P.C., Kelly, T.F., Lefebvre, W.: From the store shelf to device-level atom probe analysis: an exercise in feasibility. In: 36th International Symposium for Testing and Failure Analysis, San Jose, CA, 2011, pp. 189–197. ASM International
62. Marquis, E.A., Hu, R., Rousseau, T.: A systematic approach for the study of radiation-induced segregation/depletion at grain boundaries in steels. *J. Nucl. Mater.* **413**(1), 1–4 (2011). doi:[10.1016/j.jnucmat.2011.03.023](https://doi.org/10.1016/j.jnucmat.2011.03.023)
63. Giannuzzi, L.A., Stevie, F.: *Introduction to Focused Ion Beams, Instrumentation, Theory, Techniques and Practice*. Springer, New York, NY (2005)
64. Marquis, E.A., Geiser, B.P., Prosa, T.J., Larson, D.J.: Evolution of tip shape during field evaporation of complex multilayer structures. *J. Microsc.* **241**(3), 225–233 (2011)
65. Larson, D.J., Prosa, T.J., Geiser, B.P., Egelhoff Jr., W.L.: Effect of analysis direction on the measurement of interfacial mixing in thin metal layers with atom probe tomography. *Ultramicroscopy* **111**, 506 (2011)

66. Smith, G.D.W.: Pd as an adhesion layer for Ni and Ag. In. Personal Communication, Oxford, UK (2009)
67. Gorman, B.P.: Atom probe reconstruction refinements by pre- and post- analysis TEM structure quantification. *Microsc. Microanal.* **13**(S2), 1616–1617 (2007)
68. Arslan, I., Marquis, E.A., Homer, M., Hekmaty, M.A., Bartelt, N.C.: Towards better 3-D reconstructions by combining electron tomography and atom-probe tomography. *Ultramicroscopy* **108**, 1579–1585 (2008)
69. Gorman, B.P., Diercks, D., Kaufman, M.J., Ulfig, R.M., Lawrence, D., Thompson, K., Larson, D.J.: Atomic scale compositional and structural characterization of nanostructured materials using combined FIB, STEM, and LEAP. *Microsc. Microanal.* **12**(S2), 1720CD (2006)
70. Gorman, B.P., Diercks, D.: Cylindrical specimen geometries for sub-nm 3-D characterization of semiconductor devices. *Microsc. Microanal.* **13**(S2), 822 (2007)
71. Petersen, T.C., Ringer, S.P.: Electron tomography using a geometric surface-tangent algorithm: application to atom probe specimen morphology. *J. Appl. Phys.* **105**, 103518 (2009)
72. Antcheva, I., Ballintijn, M., Bellenot, B., Biskup, M., Brun, R., Buncic, N., Canal, P., Casadei, D., Couet, O., Fine, V., Franco, L., Ganis, G., Gheata, A., Gonzalez Maline, D., Goto, M.: ROOT—A C++ framework for petabyte data storage, statistical analysis and visualization. *Comput. Phys. Commun.* **180**, 2499–2512 (2009)
73. Williams, C.A., Marquis, E.A., Cerezo, A., Smith, G.D.W.: Nanoscale characterisation of ODS–Eurofer 97 steel: an atom-probe tomography study. *J. Nucl. Mater.* **400**, 37–45 (2010)
74. Petersen, T.C., Ringer, S.P.: An electron tomography algorithm for reconstructing 3D morphology using surface tangents of projected scattering interfaces. *Comput. Phys. Commun.* **181**, 676 (2010)
75. Giannuzzi, L.A., Schwarz, S.M.: FIB specimen preparation for STEM and EFTEM tomography. *Microsc. Microanal.* **10**(S2), 142–143 (2004)
76. Felfer, P., Alam, T., Ringer, S.P., Cairney, J.M.: A reproducible method for damage-free site-specific preparation of atom probe tips from interfaces. *Microsc. Res. Tech.* **75**, 484–491 (2012)
77. Kelly, T.F., Larson, D.J.: Atom probe tomography 2012. *Annu. Rev. Mater. Res.* **42**, 1–31 (2012)

<http://www.springer.com/978-1-4614-8720-3>

Local Electrode Atom Probe Tomography

A User's Guide

Larson, D.J.; Prosa, T.J.; Ulfig, R.M.; Geiser, B.P.; Kelly,
Th.F.

2013, XVII, 318 p. 164 illus., 54 illus. in color.,

Hardcover

ISBN: 978-1-4614-8720-3